XLIII CILAMCE
21–25, November, 2022
FOZ DO IGUAÇU – PR – BRAZIL

Numerical Analysis on Distortional Failure of Cold-Formed Steel Hat-Section Beams under Non-Uniform Bending

Carla A. L. Dib[1], Guilherme H. S. Ramos[1], Gregório S. Vieira[1]

[1]*Faculty of Civil Engineering, Federal University of Uberlândia*
Av. João Naves de Ávila, 212 – Santa Mônica, 38408-100, Uberlândia/MG, Brazil
cdib@ufu.br, guilhermeramos@ufu.br, gregorio.vieira@ufu.br

Abstract. Cold-formed steel (CFS) members stand out among steel structures notably due to their lightness, structural efficiency (high strength-to-weight ratio) and versatility. However, given their high width-to-thickness ratio, CFS are highly susceptible to instability phenomena (buckling). The objective of this research is to analyze the structural behavior of cold-formed steel hat-section beams under non-uniform bending about the major and minor-axis, regarding the risks of distortional failure. Through the Generalized Beam Theory (GBT), using the computational program GBTUL, the geometries where the distortional failure is predominant were selected, presenting: distortional modal participation (P_{dist}) greater than 85% and distortional critical buckling moments (M_{crD}) significantly below their local (M_{crL}) and global (M_{crG}) counterparts. The beams were analyzed for two end support conditions that differ only by the restriction to warping (free or prevented), and were subjected to moments at the end sections, constituting different loading hypotheses. Through the computational program ABAQUS, a shell finite element model was developed to perform the buckling analysis on the selected elements. The results obtained with the model present appropriate values and the expected behavior, indicating that it adequately simulates the elements. In addition, they demonstrate how support conditions and loading affect the distortional critical buckling moments.

Keywords: numerical analysis, cold-formed steel beams, distortional failure, non-uniform bending.

1 Introduction

Cold-formed steel (CFS) members stand out among steel structures notably due to their lightness, structural efficiency (high strength-to-weight ratio) and versatility – they are widely used in distinct segments of civil construction due to the vast variety of geometries that can be obtained in their manufacturing process.

CFS members are fabricated by press-braking or cold roll-forming thin steel sheets, with thickness ranging from 0.4 mm to 8 mm. Given their high width-to-thickness ratio, CFS are highly susceptible to instability phenomena (buckling), in which a critical force causes the structure to fail before its ultimate strength is reached. This instability phenomena can occur through local (L), distortional (D) or global (G) buckling modes, or their interactions, that happen when the critical forces corresponding to different buckling modes exhibit close values.

The member's structural performance is closely related to its geometry (cross-section dimensions and length), support conditions and loading. Therefore, according to the overall configuration, any mode of instability can be the critical mode (that is, the one corresponding to the lowest buckling load). The type of deformation presented by the structural element after buckling indicates the mode of instability that occurred: the local mode corresponds to the deformation of the cross-section elements (web, flange or lip), the distortional mode involves the deformation of the cross-section elements associated with the displacement of the edges and the global mode is characterized by the deformation of the member without changing the shape of the section, either by flexural or flexural-torsional buckling.

Among the most commonly used numerical methods for stability analysis are the Generalized Beam Theory (GBT) and the Finite Element Method (FEM).

The Generalized Beam Theory, developed by Schardt [1], is the most recent numerical method for stability

analysis and allows to quantify the percentage of participation of each instability mode of the profile, allowing a better data interpretation. Based on the GBT, Bebiano et al. [2] developed the computer program GBTUL, which allows to perform instability analysis on CFS profiles, determining the critical buckling force and the corresponding instability mode, in addition to displaying the signature curve.

The Finite Element Method allows solving a complex problem by discretizing the structure into a series of elements of simple geometry, connected together through nodal points creating a mesh (the accuracy of the method depends on the type, quantity and size of the elements). It can be used to perform different types of analysis on structures such as static, thermal, acoustic and buckling analysis, however it must be calibrated – through comparison with results obtained in analytical, numerical and experimental methods – to ensure that it reproduces adequately its behavior.

Once the stability analysis has been conducted, the design methods of CFS structural members can be performed, such as the Direct Strength Method (DSM). The method was developed by Schafer and Peköz [3], based on the studies developed by Hancock, Kwon and Bernard [4], and is adopted by the currently codified technical standards ABNT NBR 14762:2010 [5], AISI S100-16 [6] and AS/NZS 4600:2018 [7].

Hence, it is critical that the behavior related to instability phenomena be taken into account for the design and structural safety verification of CFS members. For the specific case of distortional failure in CFS hat-section beams under non-uniform bending, it is possible to observe a knowledge gap and lack of normative guidelines – the current technical standards do not present adequate formulations and provisions and there are few studies that deal with the topic.

Studies on the distortional buckling mode focus almost exclusively on columns – uniformly compressed members – and, to a lesser extent, beams under uniform bending (about the major-axis, in most cases, such as Landesmann and Camotim [8]). Bending about the minor-axis is a significantly less studied problem, even though it is widely used in practical applications. Thus, there is a need to develop studies and to deepen the knowledge on the structural performance of these elements affected by the distortional buckling mode, in order to develop, calibrate or validate methods, applicable to such scenarios.

Therefore, the objective of this research is to select a set of beams where the distortional buckling mode is predominant and to develop a finite element numerical model that adequately represents the behavior of these structural elements. In future works, the model can be used to analyze the post-buckling behavior of the members – by introducing physical and geometrical nonlinearities, such as elastoplastic material behavior and initial geometrical imperfections – and verify the applicability of the DSM in predicting failure forces.

2 Beam geometry selection

Based on the hat-section beams studied by Martins et al. [9] and through a “trial-and-error” procedure, the geometries (cross-section dimensions and length) where the distortional failure is predominant were identified by means of GBT buckling analyses performed in the program GBTUL. The program allows determining the critical buckling load, quantifying the percentage of participation of each buckling mode, as well as displaying the signature curve (a curve that relates the critical load with the profile length and provides better data interpretation). The geometries with distortional modal participation (P_D) greater than 85% were selected.

The beams were analyzed for two simple support conditions, named SCA (Support Condition A) and SCB (Support Condition B). The SCA beams present free major and minor-axis bending, prevented end cross-section torsional rotations and free warping (longitudinal displacement). The SCB beams differ only by also presenting prevented warping.

The beams were subjected to major-axis (H_M) and minor-axis (H_m) bending, with lips under compression in the latter case (worst condition), through the application of moments at the end sections, M_1 and M_2, establishing three load hypotheses (moment gradients): $\psi = 1$, $\psi = 0$ and $\psi = -1$, where $\psi = M_2/M_1$, and M_1 is constant.

In order to avoid the interaction between different buckling modes, geometries with distortional critical buckling moments (M_{crD}) significantly below their local (M_{crL}) and global (M_{crG}) counterparts were selected, presenting M_{crL}/M_{crD} and $M_{crG}/M_{crD} > 2$.

The cross-section elements – web (b_w), flange (b_f), lip (b_l) and thickness (t) – of hat-section members are illustrated in Fig. 1 and the geometric parameters of the selected beams are presented in Tab. 1. Calculations were performed considering the material with elastic modulus $E = 210\text{GPa}$ and Poisson's ratio $\nu = 0{,}3$.

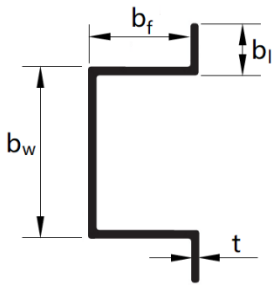

Figure 1. Cross-section elements of hat-section members.

Table 1. Cross-section dimensions for selected beams.

Beam	b_w (mm)	b_f (mm)	b_l (mm)	t (mm)
H1	120	80	10	2.5
H2	125	80	10	3.0
H3	130	80	10	2.5
H4	135	90	10	3.0
H5	140	90	10	2.5
H6	150	120	10	3.5
H7	160	90	10	3.0
H8	160	100	10	2.5
H9	200	120	10	3.0
H10	210	110	10	3.5

The lengths (L), distortional critical buckling moments (M_{crD}), M_{crL}/M_{crD} and M_{crG}/M_{crD} relations, and distortional modal participations (P_D) for the different moment gradients are presented in Tab. 2 to 4.

Table 2 – Critical lengths, M_{crD} and their relations, and modal participation – $\psi = 1$.

Beam	SCA					SCB				
	L (cm)	M_{crD} (kNcm)	$\frac{M_{crL}}{M_{crD}}$	$\frac{M_{crG}}{M_{crD}}$	P_D (%)	L (cm)	M_{crD} (kNcm)	$\frac{M_{crL}}{M_{crD}}$	$\frac{M_{crG}}{M_{crD}}$	P_D (%)
H_M1	35	1033.20	3.08	50.49	95.16	60	1502.31	2.16	26.77	92.11
H_m1		479.55	7.49	29.91	95.13		695.71	5.21	28.03	95.12
H_M2	30	1670.55	3.50	53.93	94.82	45	2489.66	2.41	36.42	91.56
H_m2		756.13	8.37	33.71	93.00		1142.19	5.63	39.60	93.30
H_M3	40	1118.88	3.11	39.81	96.26	55	1652.80	2.14	32.26	91.97
H_m3		466.17	7.56	27.75	94.73		711.50	5.04	38.37	93.54
H_M4	45	1621.23	3.44	36.82	96.67	50	2350.51	2.42	46.52	91.67
H_m4		711.60	8.68	23.45	96.18		1104.55	5.71	48.71	94.11
H_M5	40	1060.39	3.09	62.23	95.60	60	1566.90	2.14	42.40	91.86
H_m5		462.13	7.49	40.85	94.65		695.37	5.06	48.19	94.28
H_M6	50	1881.61	3.85	71.36	96.43	45	3200.50	2.37	117.14	88.48
H_m6		972.64	10.07	34.67	97.69		1857.26	5.46	89.28	94.99
H_M7	35	1872.62	3.57	66.14	95.97	45	2994.96	2.29	56.66	90.68
H_m7		723.24	8.18	53.27	90.16		1208.33	5.01	77.03	88.88
H_M8	30	1315.76	2.55	138.83	89.50	65	1594.07	2.15	55.34	91.94
H_m8		591.97	5.67	90.89	88.65		678.72	5.02	67.58	93.73
H_M9	40	1759.25	3.52	149.71	94.85	55	2747.71	2.32	114.89	90.26
H_m9		715.27	7.88	113.17	90.06		1156.70	5.02	147.97	89.87
H_M10	50	2937.24	4.00	57.44	96.51	65	4015.39	2.99	56.30	94.61
H_m10		989.29	9.44	56.17	90.58		1399.16	6.78	93.83	89.75

Table 3 – Critical lengths, M_{crD} and their relations, and modal participation – $\psi = 0$.

Beam	SCA					SCB				
	L (cm)	M_{crD} (kNcm)	$\frac{M_{crL}}{M_{crD}}$	$\frac{M_{crG}}{M_{crD}}$	P_D (%)	L (cm)	M_{crD} (kNcm)	$\frac{M_{crL}}{M_{crD}}$	$\frac{M_{crG}}{M_{crD}}$	P_D (%)
H_M1	35	1676.32	2.21	57.76	89.70	95	1946.74	2.14	15.50	91.66
H_m1		815.83	5.10	33.07	92.75		921.44	5.07	16.04	94.31
H_M2	30	2743.06	2.51	60.95	89.07	70	3399.60	2.22	20.72	89.72
H_m2		1296.14	5.68	36.99	90.64		1563.57	5.23	22.68	92.13
H_M3	40	1757.33	2.28	47.04	90.98	95	2116.16	2.15	15.89	91.62
H_m3		770.25	5.28	31.59	92.63		920.69	4.99	18.88	92.90
H_M4	45	2389.54	2.69	46.37	92.14	75	3266.55	2.19	27.96	89.55
H_m4		1113.43	6.40	28.19	94.22		1545.45	5.17	29.33	92.96
H_M5	40	1700.43	2.24	72.03	90.02	105	1995.77	2.15	20.44	91.70
H_m5		779.63	5.14	45.55	92.44		894.33	5.04	23.23	93.75
H_M6	50	2793.30	3.03	89.21	92.52	60	4499.96	2.22	88.00	89.09
H_m6		1535.54	7.42	41.31	95.57		2539.57	5.12	69.49	93.21
H_M7	35	3045.06	2.52	75.49	89.37	75	3912.27	2.19	29.34	88.98
H_m7		1227.90	5.63	59.03	87.91		1548.42	4.93	41.00	89.45
H_M8	45	1714.05	2.28	87.99	90.28	105	2102.77	2.09	30.21	90.79
H_m8		750.20	5.17	60.06	92.09		910.04	4.82	36.60	92.80
H_M9	40	2871.71	2.49	170.23	88.21	95	3516.64	2.25	56.51	89.50
H_m9		1223.62	5.47	124.46	87.71		1444.06	5.06	75.21	90.77
H_M10	50	4336.51	3.03	72.21	92.07	65	6583.36	2.29	64.45	88.36
H_m10		1541.48	6.98	67.81	88.48		2392.31	5.05	103.74	87.76

Table 4 – Critical lengths, M_{crD} and their relations, and modal participation – $\psi = -1$.

Beam	SCA					SCB				
	L (cm)	M_{crD} (kNcm)	$\frac{M_{crL}}{M_{crD}}$	$\frac{M_{crG}}{M_{crD}}$	P_D (%)	L (cm)	M_{crD} (kNcm)	$\frac{M_{crL}}{M_{crD}}$	$\frac{M_{crG}}{M_{crD}}$	P_D (%)
H_M1	150	1431.06	2.71	5.67	91.80	215	1867.17	3.26	5.62	88.94
H_m1		670.64	2.04	5.14	94.47		884.79	2.10	7.88	93.94
H_M2	95	2446.41	2.92	10.29	90.78	185	3018.97	3.33	5.95	89.13
H_m2		1117.44	2.07	9.81	93.34		1375.90	2.08	8.94	92.82
H_M3	235	1465.77	3.46	2.63	92.54	245	1931.91	3.79	4.67	89.58
H_m3		620.87	2.05	2.81	93.49		835.65	2.09	7.59	93.05
H_M4	85	2454.36	2.78	18.88	90.63	185	2993.92	3.01	8.89	90.63
H_m4		1160.53	2.08	17.12	93.67		1400.25	2.10	12.79	93.72
H_M5	195	1435.23	2.87	5.53	91.85	245	1898.12	3.32	7.00	90.18
H_m5		631.30	2.05	5.56	94.35		847.64	2.06	10.83	93.50
H_M6	50	3500.39	2.55	105.22	85.92	115	4619.38	2.35	40.99	87.63
H_m6		2109.26	2.37	67.20	89.99		2601.83	2.22	43.90	92.76
H_M7	225	2440.18	3.60	3.58	93.37	265	3122.07	4.26	5.26	91.57
H_m7		929.30	2.07	4.54	90.28		1205.92	2.11	10.24	90.73
H_M8	235	1443.89	3.00	5.88	92.39	275	1912.09	3.39	8.58	90.87
H_m8		605.73	2.05	6.38	93.80		816.15	2.04	14.29	92.94
H_M9	145	2478.51	3.04	22.39	91.99	275	3034.90	3.45	13.79	91.39
H_m9		998.44	2.09	26.26	92.19		1223.16	2.09	25.35	91.49
H_M10	185	3857.10	3.69	8.96	92.98	285	4765.63	4.34	8.21	92.74
H_m10		1351.54	2.12	12.97	88.54		1681.22	2.10	18.50	87.67

In addition, Fig. 2 illustrates the signature curves of beam H4, exhibiting the behavior of the distortional critical buckling moment as a function of length (logarithmic scale), for the different loading hypotheses.

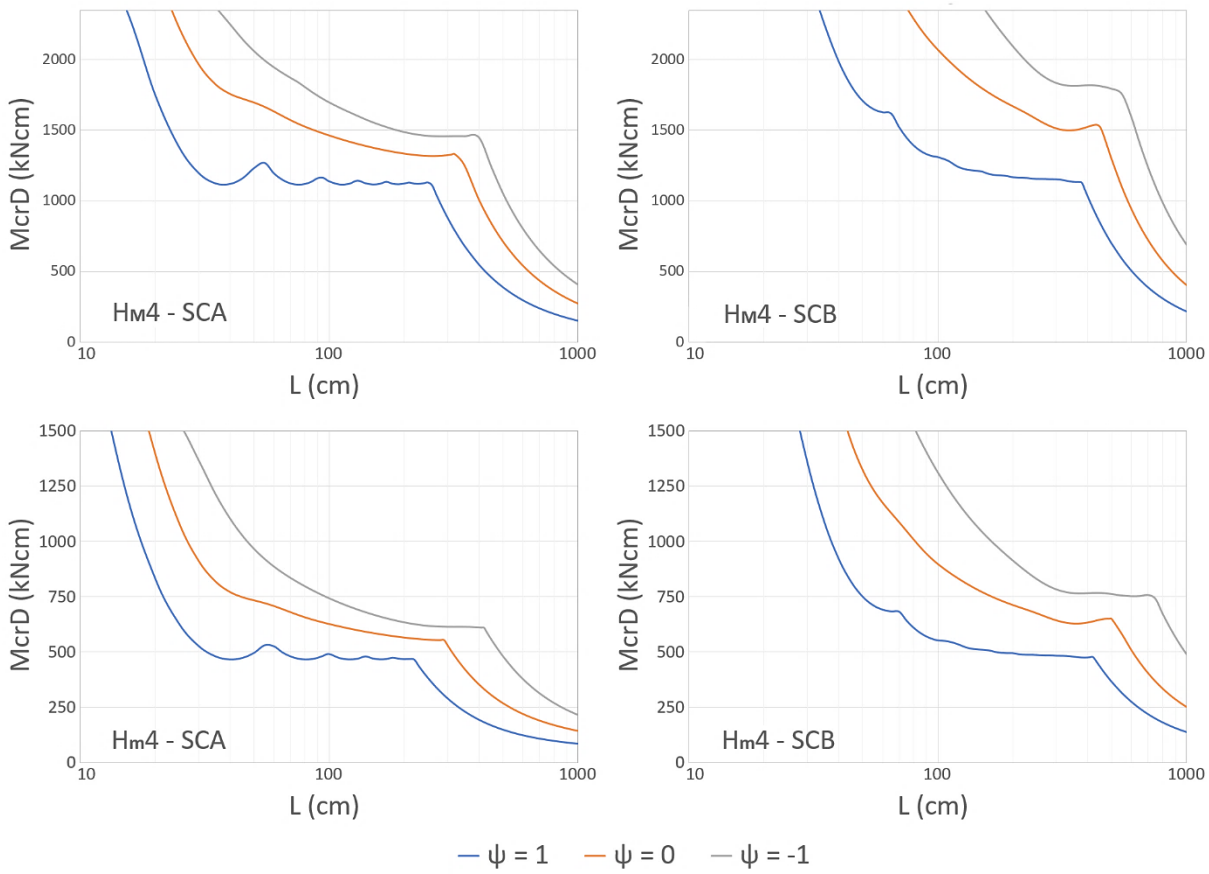

Figure 2. Signature curves ($M_{crD} \times L$) for different moment gradients (ψ).

3 Shell finite element analysis

A numerical model was developed to perform buckling analyses using the Finite Element Method (FEM) through the program ABAQUS.

Since the plates that constitute CFS members have small thickness, a shell element denominated S8R was chosen for the model: an 8-node quadrilateral element with reduced integration. In order to estimate the most appropriate mesh refinement, ensuring an accurate solution and an optimized analysis processing time, a convergence study was performed and a 5 mm × 5 mm mesh was adopted.

The SCB beams, that differs by the restriction to warping, were modeled by attaching rigid plates to their end cross-sections (elastic modulus $E = 2100$ GPa) and by applying transverse displacement constraints and axial rotation constraints directly at the plates. Likewise, at the beam mid-web mid-length point an axial displacement constraint was applied. For this support condition, the unitary moments were applied directly at the rigid plates.

4 Results

Through the linear perturbation analysis procedure, the critical buckling moment values and the corresponding instability mode are obtained. The buckling analysis is performed using the eigenvalue method (to determine the critical force) and the eigenvector method (to determine the buckling mode). The values presented correspond to the smallest eigenvalue (and respective eigenvector), however, the method allows calculating the other possible solutions for the system.

The critical buckling moments obtained via the numerical model (M_{Abq}) and their relation with the critical buckling moments obtained via GBTUL (M_{GBTUL}) – shown in Tab. 2 to 4 as M_{crD} – are presented in Tab. 5 and 6, for the different moment gradients.

Table 5 – Critical buckling moments M_{Abq} and their relation with M_{GBTUL} – SCA.

Beam	$\psi = 1$		$\psi = 0$		$\psi = -1$	
	M_{Abq} (kNcm)	M_{GBTUL}/M_{Abq}	M_{Abq} (kNcm)	M_{GBTUL}/M_{Abq}	M_{Abq} (kNcm)	M_{GBTUL}/M_{Abq}
H_M1	1022.10	1.01	1640.70	1.02	1398.40	1.02
H_m1	473.68	1.01	798.35	1.02	657.01	1.02
H_M2	1642.90	1.02	2665.10	1.03	2385.70	1.03
H_m2	741.88	1.02	1257.90	1.03	1090.90	1.02
H_M3	1109.30	1.01	1724.00	1.02	1403.00	1.04
H_m3	461.96	1.01	756.00	1.02	599.02	1.04
H_M4	1607.10	1.01	2342.00	1.02	2397.90	1.02
H_m4	705.41	1.01	1091.70	1.02	1134.60	1.02
H_M5	1051.90	1.01	1670.00	1.02	1399.20	1.03
H_m5	457.68	1.01	765.53	1.02	617.79	1.02
H_M6	1868.20	1.01	2746.00	1.02	3399.10	1.03
H_m6	963.99	1.01	1507.40	1.02	2042.30	1.03
H_M7	1847.30	1.01	2970.90	1.02	2342.20	1.04
H_m7	712.71	1.01	1197.80	1.03	898.71	1.03
H_M8	1293.80	1.02	1687.70	1.02	1403.50	1.03
H_m8	579.62	1.02	738.59	1.02	591.78	1.02
H_M9	1740.80	1.01	2812.20	1.02	2434.90	1.02
H_m9	706.54	1.01	1198.60	1.02	982.88	1.02
H_M10	2913.90	1.01	4258.30	1.02	3761.70	1.03
H_m10	980.49	1.01	1512.00	1.02	1320.40	1.02

Table 6 – Critical buckling moments M_{Abq} and their relation with M_{GBTUL} – SCB.

Beam	$\psi = 1$		$\psi = 0$		$\psi = -1$	
	M_{Abq} (kNcm)	M_{GBTUL}/M_{Abq}	M_{Abq} (kNcm)	M_{GBTUL}/M_{Abq}	M_{Abq} (kNcm)	M_{GBTUL}/M_{Abq}
H_M1	1469.00	1.02	1917.20	1.02	1806.60	1.03
H_m1	682.21	1.02	898.62	1.03	852.20	1.04
H_M2	2415.70	1.03	3354.60	1.01	2915.20	1.04
H_m2	1106.40	1.03	1512.70	1.03	1317.00	1.04
H_M3	1615.90	1.02	2084.90	1.01	1872.90	1.03
H_m3	695.85	1.02	897.72	1.03	808.68	1.03
H_M4	2288.60	1.03	3237.70	1.01	2894.50	1.03
H_m4	1074.10	1.03	1499.20	1.03	1340.90	1.04
H_M5	1535.00	1.02	1971.00	1.01	1841.10	1.03
H_m5	681.41	1.02	873.85	1.02	818.85	1.04
H_M6	3088.50	1.04	4580.80	0.98	4699.30	0.98
H_m6	1782.70	1.04	2458.30	1.03	2499.70	1.04
H_M7	2898.40	1.03	3877.40	1.01	3020.50	1.03
H_m7	1165.60	1.04	1502.00	1.03	1165.80	1.03
H_M8	1564.30	1.02	2084.30	1.01	1858.20	1.03
H_m8	666.01	1.02	889.76	1.02	790.40	1.03
H_M9	2673.20	1.03	3513.30	1.00	2956.20	1.03
H_m9	1122.90	1.03	1409.40	1.02	1181.60	1.04
H_M10	3934.70	1.02	6650.40	0.99	4635.80	1.03
H_m10	1369.20	1.02	2316.10	1.03	1624.80	1.03

From the results, it is possible to observe that the greatest differences between the moments obtained by the two distinct methods are approximately 4%, which indicates that the numerical model adequately simulates the profiles behavior. The deformed configuration of the beams also presents the expected aspect – distorted cross-

section elements associated with the displacement of the edges – in the different support conditions and loading hypotheses, as shown in Fig. 3 for the beam H2, confirming the suitability of the developed model.

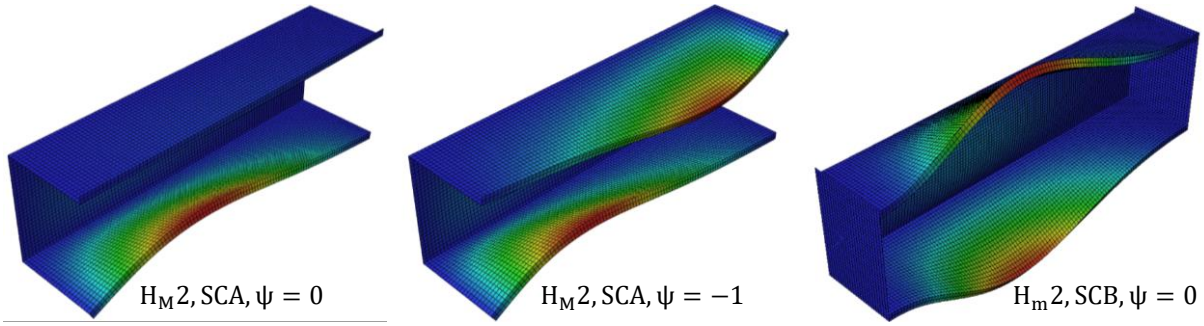

Figure 3. Distortional buckling: deformed configurations.

5 Conclusions

From the results, shown in Tab. 2 to 6 and in Fig. 1, it is possible to observe how the member's structural performance is affected by its geometry, support conditions and loading: (i) beams subjected to non-uniform bending present higher distortional critical buckling moments when compared to beams subjected to uniform bending and (ii) SCB beams have higher distortional critical buckling moments than SCA beams. For the same length, the values increase in the sequence $\psi = 1 \rightarrow 0 \rightarrow -1$ and SCA $\rightarrow$ SCB, as observed by Yu and Schafer [10]. This behavior can be observed either in beams subjected to bending around the major or minor-axis.

Moreover, based on the highest difference between the distortional critical buckling moments obtained through FEM and GBT, shown in Tab. 5 and 6, and based on the deformed configuration of the beams illustrated in Fig. 3, it is possible to conclude that the numerical model developed in this study adequately simulates the structural behavior of CFS hat-section beams under non-uniform bending about the major and minor-axis, regarding the risks of distortional failure.

Authorship statement. The authors hereby confirm that they are the sole liable persons responsible for the authorship of this work, and that all material that has been herein included as part of the present paper is either the property (and authorship) of the authors, or has the permission of the owners to be included here.

References

[1] R. Schardt, "Generalized beam theory – an adequate method for coupled stability problems". *Thin-Walled Structures*, v.19, n.2-4, p.161-180, 1994.
[2] R. Bebiano, D. Camotim and R. Gonçalves, "GBTUL 2.0 – a second generation code for the GBT-based buckling and vibration analysis of thin-walled members". *Thin-Walled Structures*, v.124, p.235-253, 2018.
[3] B. W. Schafer and T. Peköz, "Direct strength prediction of cold-formed steel members using numerical elastic buckling solutions". In: *Proceedings of the 14th international specialty conference on cold-formed steel structures*, p.69-76, 1998.
[4] G. J. Hancock, Y. B. Kwon and E. S. Bernard, "Strength design curves for thin-walled sections undergoing distortional buckling". *Journal of Constructional Steel Research*, v.31, n.2-3, p.169-186, 1994.
[5] Brazilian Association of Technical Standards, "NBR 14762 – Design of cold-formed steel structures". 2010.
[6] American Iron and Steel Institute. "AISI S100-16 – North American Specification for the design of cold-formed steel structural members". 2016.
[7] Australian / New Zealand Standards. "AS/NZS 4600 – Cold-formed steel structures". 2018.
[8] A. Landesmann and D. Camotim, "Distortional failure and DSM design of cold-formed steel lipped channel beams under elevated temperatures". *Thin-Walled Structures*, v.98, p.75-93, 2016.
[9] A. D. Martins, A. Landesmann, D. Camotim and P. B. Dinis, "Distortional failure of cold-formed steel beams under uniform bending: Behaviour, strength and DSM design". *Thin-Walled Structures*, v.118, p.196-213, 2017.
[10] C. Yu and B. W. Schafer, "Distortional buckling of cold-formed steel members in bending". *American Iron and Steel Institute (AISI)*, 2005.